6

Parallel plate counters

6.1 Charge induction on conductors

A positive charge placed between two conducting electrodes induces on both a negative charge distribution with shape and amplitude that depend on geometry. Figure 6.1 shows schematically the induction profile for two positions of a positive charge placed at equal distance (left) or asymmetrically between two electrodes (right). Intuitively, and as can be inferred from the image charges model, the induction profile is narrower and higher when the charge is closer to the electrode.

Electrons and ions released within a gaseous counter by ionizing events drift towards anode and cathode, respectively, under the effect of the applied electric field. For moderate fields, before the appearance of inelastic collision processes and in the absence of capture and recombination, the final outcome is the collection at the electrodes of all charges; during the drift, induced signals appear on the electrodes, with polarity and time structure that depend on the counter geometry, field strength and mobility of the charges.

The motion of ions and electrons towards the electrodes increases their surface charges, the cathode towards more negative and the anode towards more positive values; the signals detected on a load are, however, opposite in polarity. Suppose indeed that the cathode is connected to the voltage through a resistor. An increase of the negative charge on the electrode implies an inflow of electrons, or, from the definition of electric current, an outflow of positive charges; the detected voltage difference is therefore positive. This is often confusing, so the reader could memorize the golden rule of induced signal formation: 'A positive charge moving towards an electrode generates an induced positive signal; if it moves away from the electrode, the signal is negative', and similarly for negative charges, with opposite signs.

Methods to compute the currents induced by moving charges on conductors of arbitrary shape were developed to describe the signal formation in vacuum tubes

https://doi.org/10.1017/9781009291200.008 Published online by Cambridge University Press

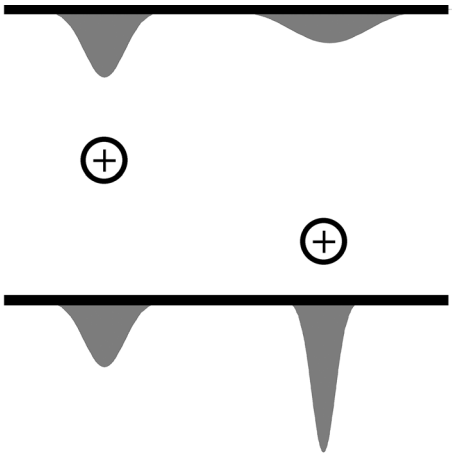

Figure 6.1 Profiles of charges induced on electrodes by a positive charge in two different positions.

(Shockley, 1938; Ramo, 1939); named the Ramo theorem, the basic equation can be written as:

$$i = E_v e v,$$

where i is the instantaneous current flowing in a given electrode due to the motion of a single electron of charge e and velocity v and E_v is the component in the direction of the electric field which would exist at the electron's position with that electron removed, the electrode raised to unit potential and all other electrodes grounded.

Standard methods of electrostatics can be used to compute analytically the induced signal distributions on electrodes with a given geometry (Durand, 1966; Morse and Feshbach, 1953; Mathieson and Smith, 1988). A general expression can be written to estimate the time development of signals for the charges induced by the system of ions located in known positions, then computing the signal development as the increment (or decrement) of induced charge on each electrode during the motion along the field lines of the various primary charges, with the appropriate velocity. For complex geometries this becomes rather tedious, and approximate numerical solutions are generally preferred; web-based programs are also available for this calculation (Veenhof, 1998; Veenhof, 2002).

6.2 Signals induced by the motion of charges in uniform fields

For parallel electrode geometry, expressions for the induced signals can be obtained from simple energy conservation principles. Consider a system composed

https://doi.org/10.1017/9781009291200.008 Published online by Cambridge University Press

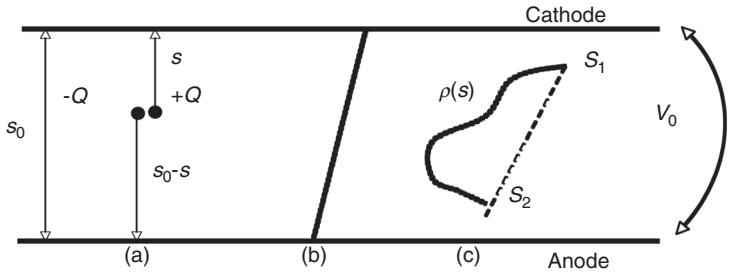

Figure 6.2 Point-like ionization (a), extended ionization trail (b) and localized trail (c).

of two electrodes, anode and cathode, at a distance s_0 and difference of potential V_0 (Figure 6.2).

Assuming that the work done by the field to move the charge Q by ds is equal to the change in electrostatic energy stored by the system, one can write for the incremental induced charge, see for example Franzen and Cochran (1956):

$$\mathrm{d}q = Q\frac{\mathrm{d}V}{V_0} = Q\frac{\mathrm{d}s}{s_0}. \tag{6.1}$$

For a charge Q drifting in a uniform electric field with constant velocity w, the current delivered by the source of potential is then:

$$i = \frac{\mathrm{d}q}{\mathrm{d}t} = \frac{Q}{s_0}\frac{\mathrm{d}s}{\mathrm{d}t} = \frac{Q}{s_0}w \tag{6.2}$$

and the corresponding charge is:

$$q(t) = \frac{Q}{s_0}wt. \tag{6.3}$$

At the same time, a current equal and opposite in sign appears on the anode; the motion of a negative charge has the same effect with inverted sign. The currents cease at the moment the charges reach an electrode; integration of expression (6.1) provides the total induced charge:

$$q = Q\frac{s}{s_0}, \tag{6.4}$$

reducing to $q = Q$ if the charge is released on one electrode surface and drifts through all the gap.

Suppose now that a pair of charges of opposite sign is released at a distance s from the cathode (Figure 6.2a). At the moment of creation, and in fact forever in the absence of motion, the induced charges on each electrode, equal and opposite,

https://doi.org/10.1017/9781009291200.008 Published online by Cambridge University Press

cancel out. In the presence of a field, and because of their different mobility, electrons and ions are collected at a different rate; the relative contributions to the total induced signal depend on the initial position of production. In the case of an ionization event releasing at time $t = 0$ and position s equal amounts of electrons and ions of charge $-Q$ and $+Q$, the time development of the induced charge (from (6.3)) can be written as:

$$q(t) = Q\frac{w^+ t}{s_0} + Q\frac{w^- t}{s_0}, \tag{6.5}$$

where w^+ and w^- are drift velocities of ions and electrons; the corresponding voltage difference across the capacitor is given by $V(t) = q(t)/C$. Both terms in expression (6.5) have values restricted to the maximum time of drift before collection, T^+ and T^- for ions and electrons respectively. The total induced charge after full collection is then:

$$q_T = Q\frac{w^+ T^+}{s_0} + Q\frac{w^- T^-}{s_0} = Q\frac{s}{s_0} + Q\frac{s - s_0}{s_0} = Q.$$

Figure 6.3 gives an example of the time development of the induced charge and current on the cathode on a parallel plate ionization counter for equal amounts of electrons and ions released mid-way between two electrodes. For illustration purposes the mobility of electrons has been assumed to be only ten times that of ions (they differ in fact by three orders of magnitude). Signals on anodes are equal and opposite in sign.

The previous expressions permit us to compute the induced charge and current for the case of extended tracks, as those produced by charged particles traversing the gap (Figure 6.2b). Suppose the ionized trail to be perpendicular to the

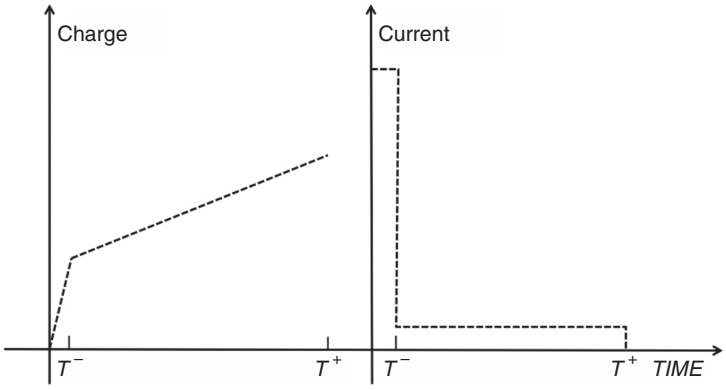

Figure 6.3 Charge and current induced on cathodes by the drift of electrons and ions.

https://doi.org/10.1017/9781009291200.008 Published online by Cambridge University Press

electrodes, with uniform charge density $\rho = Q / s_0$. Considering for the time being only one species of released charges, after a time t a segment of track of length wt will have disappeared, collected by the electrode. The induced current at time t can thus be written (in analogy with expression (6.2)):

$$i = \frac{w}{s_0} \int_0^{s_0 - wt} \rho \, \mathrm{d}s = \frac{w}{s_0} \rho \, (s_0 - wt) = \frac{wQ}{s_0} \left(1 - \frac{w}{s_0} t \right), \tag{6.6}$$

and the corresponding charge:

$$q(t) = \int_0^t i \, \mathrm{d}t = \frac{wQ}{s_0} t \left(1 - \frac{wt}{2s_0} \right). \tag{6.7}$$

The induced charge signal rises to a maximum equal to $Q/2$, reached at the time of full collection $T = s_0/w$ (Fig 6.4); charges of opposite polarity induce a signal described by expressions (6.6) and (6.7), with the same sign and with the appropriate value of the drift velocity; the two contributions add up as in previous examples. In the case of inclined tracks, the induction process is described by the same expressions, substituting for the real charge density its projection on the normal to the electrodes.

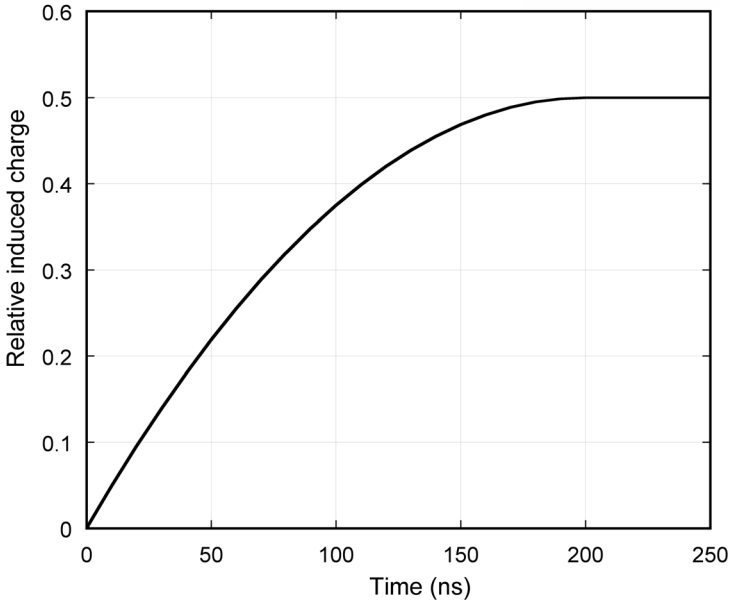

Figure 6.4 Electron-induced charge on cathodes by an extended track.

https://doi.org/10.1017/9781009291200.008 Published online by Cambridge University Press

The induced charge signal can be computed in the general case of non-uniform ionization. Consider, for example, a charged particle (say, a photoelectron) produced and coming to rest between two positions at distance s_1 and s_2 from one electrode, and producing a trail with ionization density (projected on the coordinate s perpendicular to the electrodes) given by $\rho(s)$ (Figure 6.2c). The charge induced on the electrodes from the time of production to the moment the first electron reaches the anode is given by (see (6.3)):

$$q(t) = \frac{wt}{s_0} \int_{s_1}^{s_2} \rho(s) \mathrm{d}s,$$

and the corresponding current:

$$i = \frac{w}{s_0} \int_{wt}^{s_2} \rho(s)\, \mathrm{d}s,$$

where one can see that the slope of the induced signal before collection depends only on the total ionization charge (and not on its detailed distribution). From the moment collection starts, $t_1 = s_1/w$, and before collection of the last electron the induced current is:

$$i = \frac{w}{Cs_0} \int_{wt}^{s_2} \rho(s)\, \mathrm{d}s$$

and:

$$\frac{\mathrm{d}i}{\mathrm{d}t} = \frac{w^2}{s_0} \rho(wt),$$

where $\rho(wt)$ is the density of ionization at a distance wt-s_1 from the end of the track, measured along s; the observation of the induced charge profile is in principle providing the (projected) ionization energy loss density along the track. The same considerations apply to the signals induced by positive ions, although at a much longer time scale.

6.3 Analytical calculation of charge induction

A powerful method for evaluating the static distribution of induced charges on electrodes is based on Green's reciprocation theorem, also called the Gauss identity, stating that when a set of charges $Q_a, Q_b, \ldots (Q'_a, Q'_b, \ldots)$ is placed on insulated conductors *a, b,* ..., they acquire the potentials $V_a, V_b, \ldots (V'_a, V'_b, \ldots)$ so that the following relationship is satisfied:

https://doi.org/10.1017/9781009291200.008 Published online by Cambridge University Press

$$\sum Q'_i V_i = \sum Q_i V'_i \tag{6.8}$$

with the sum extended to all conductors. It is assumed that the variation of potentials in all electrodes due to deposition or induction of charges is negligible compared to the ones previously existing; this is verified in practice for the charge densities encountered in ionization and proportional chambers. A solution to the induction problem can then be found by writing expression (6.8) for a set of suitably chosen initial conditions.

As an application of Green's theorem, consider the case of a charge q placed at a point P close to a single conductor of arbitrary shape. Let V be the potential at the point P, and Q the induced charge to be evaluated on the conductor assumed at potential $V = 0$. As a second equilibrium state, consider the case of $q = 0$, induced charge Q' and potentials V' and V'_0 at P and on the conductor respectively. The two sets of conditions can be written as follows:

$$(q, Q);(V, 0),$$
$$(0, Q');(V', V'_0);$$

from expression (6.8) one has then:

$$qV' + QV'_0 = 0$$

and therefore:

$$Q = -\frac{V'}{V'_0} q. \tag{6.9}$$

The induced charge on the conductor at ground potential can then be computed, knowing the potential V' produced, in the point P and with q removed, by the conductor raised at the potential V'_0. This is simple for the case of a charge at distance r from a spherical conductor of radius R:

$$V' = \frac{R}{r} V'_0,$$

and therefore:

$$Q = -\frac{R}{r} q, \quad r > R.$$

For an infinite plane conductor, $Q = -q$, as can be deduced from the previous expression for r, $R \to \infty$.

Similarly, consider a charge $+q$ placed between two parallel and infinite electrodes at potentials V_1 and V_2, at distances s and $s_0 - s$ respectively (s_0 being the total gap, see Figure 6.5). We can choose the following three sets of conditions:

https://doi.org/10.1017/9781009291200.008 Published online by Cambridge University Press

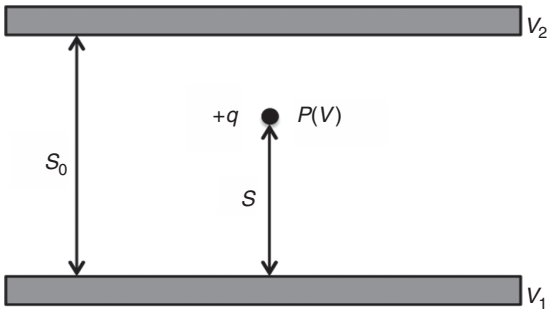

Figure 6.5 Positive charge placed between two parallel electrodes: parameter definition.

$$(q, Q_1, Q_2);(V, 0, 0),$$
$$(0, Q_1', Q_2');(V', V_1', 0),$$
$$(0, Q_1'', Q_2'');(V'', 0, V_2'');$$

applying Green's theorem to pairs of sets:

$$Q_1 = \frac{V'}{V_1'} q = -\frac{s_0 - s}{s_0} q,$$
$$Q_2 = \frac{V''}{V_2''} q = -\frac{s}{s_0} q, \tag{6.10}$$

where the linear dependence of the potential between two parallel electrodes, in the absence of the charge q, has been taken into account:

$$\frac{V - V_1}{V_2 - V_1} = \frac{s}{s_0}$$

and similar expressions for the other cases.

Note that in the limiting case of a charge placed infinitely close to one conductor $s \to 0$, $Q_1 \to -q$ and $Q_2 \to 0$. Also, if one brings to infinite distance the electrode 2 ($s_0 \to \infty$), as expected $Q_1 \to -q$ and $Q_2 \to 0$.

For infinite parallel electrodes, the time development of induced charges can be easily computed from energy conservation principles. In the general case of complex geometries, for example with segmented electrodes (strips or wires), and for distributions of charges, one has to resort to more sophisticated electrostatic algorithms. The method of image charges can be used to get an intuitive picture of the induction process, and in some simple cases to compute the distribution of

https://doi.org/10.1017/9781009291200.008 Published online by Cambridge University Press

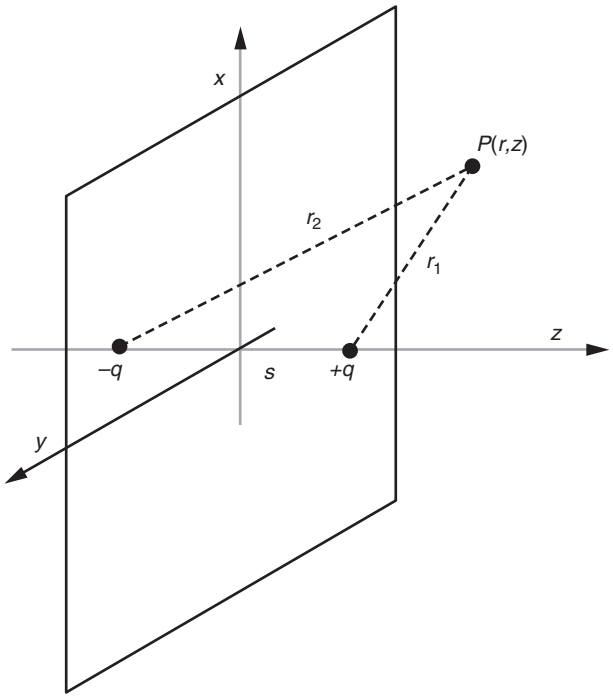

Figure 6.6 Image charge method: definition of geometry.

induced charges. Consider the case of a positive point charge q placed at a distance s from an infinite plane conductor. Elementary electrostatics suggests that one can replace the conductor with an image charge $-q$ placed symmetrically to q (Figure 6.6); indeed, the central plane in this case is equi-potential.

The potential on any point in space of coordinates *(x, y, z)* can then be written as:

$$\begin{aligned} V &= \frac{q}{4\pi\varepsilon_0}\left(\frac{1}{\sqrt{x^2+y^2+(z-s)^2}} - \frac{1}{\sqrt{x^2+y^2+(z+s)^2}}\right) \\ &= \frac{q}{4\pi\varepsilon_0}\left(\frac{1}{\sqrt{\rho^2+(z-s)^2}} - \frac{1}{\sqrt{\rho^2+(z+s)^2}}\right), \end{aligned} \tag{6.11}$$

with $\rho = \sqrt{x^2+y^2}$. The corresponding surface charge density on the conductor is then given by:

https://doi.org/10.1017/9781009291200.008 Published online by Cambridge University Press

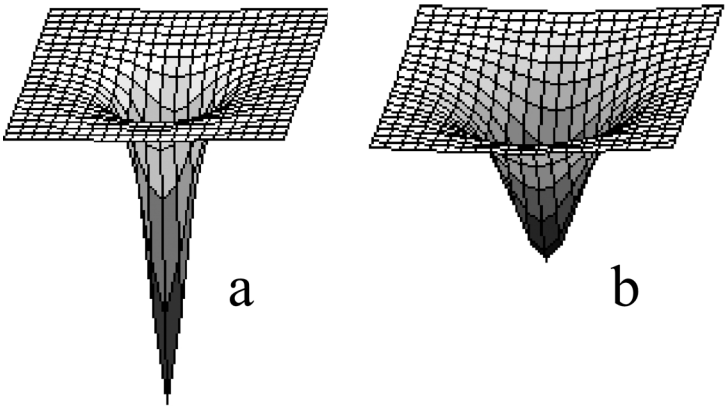

Figure 6.7 Charge induction profile on a conducting plane for two values of the distance of a charge from the plane.

$$\sigma(x,y) = \sigma(\rho,\theta) = -\varepsilon_0 \left(\frac{\partial V}{\partial z}\right)_{z=0} = -\frac{qs}{2\pi(\rho^2+s^2)^{3/2}} = -\frac{qs}{2\pi l^3}, \qquad (6.12)$$

where l is the distance of a point on the conductor from the charge q. Peaked in front of q, the induced charge distribution has a shape that depends on the distance s from the plane (Figure 6.7).

The total induced charge is obtained by integration of the previous expression and is obviously equal and opposite in sign to the original charge:

$$Q = \int \sigma(x,y)\mathrm{d}x \ \ \mathrm{d}y = -q.$$

The charge density in an arbitrary point (x, y) on the plane can be estimated from expression (6.12), as a function of s, as shown for example in Figure 6.8, computed for $y = 0$ and several values of x. Note that the induced charge density decreases towards negative values at the approach of q to the plane, but returns to zero when the charge reaches it ($s = 0$). For $x = 0$, the expression of charge density has a singularity, with the corresponding function tending to infinity (however, its integral equals $-q$ as previously stated). This behaviour corresponds to the general statement that, however large the induced charge on a surface element is, its final value after full collection of the moving charge is different from zero only if some charge is collected by that element.

Differentiation of (6.12) with respect to s provides the following expression, which can be interpreted as the current density at the point (x, y) generated by the uniform approach of the charge q to the conductor:

https://doi.org/10.1017/9781009291200.008 Published online by Cambridge University Press

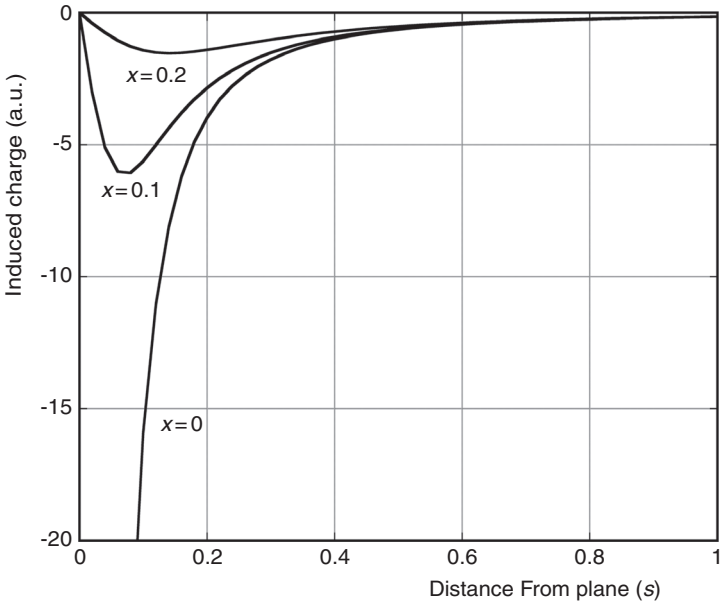

Figure 6.8 Charge induction profile as a function of distance of the charge from the (x, y) plane, for several values of x at $y = 0$.

$$i(s) = -\frac{q}{2\pi}\frac{(x^2 - 2s^2)}{(x^2 + s^2)^{5/2}}.$$

In the case of a segmented electrode, the fraction of charge induced on each segment can be computed by integration of the previous expression between the appropriate boundaries. Let us first consider the case of an electrode made of concentric rings, centred on the origin. The charge induced on the ring between r_1 and r_2 is then:

$$Q_{12} = \int_0^{2\pi} \mathrm{d}\theta \int_{\rho_1}^{\rho_2} \sigma(\rho, \theta)\mathrm{d}\rho = -\frac{q}{s}\left(\frac{\rho_2}{\sqrt{\rho_2^2 + s^2}} - \frac{\rho_1}{\sqrt{\rho_1^2 + s^2}}\right).$$

In Figure 6.9 the charge induced on concentric rings of unitary thickness is shown as a function of their radius, for three values of the distance s. For values of s larger than the minimum ring radius, the induced charge profile is peaked at increasing distances from the origin, reflecting the larger solid angle of those rings.

Expression (6.12) can be integrated on strips parallel to the y coordinate, between the coordinates x_1 and x_2 :

$$Q_{12} = \int_0^{\infty} \mathrm{d}y \int_{x_1}^{x_2} \sigma(x, y)\mathrm{d}x = -\frac{q}{\pi}\left(\arctan\frac{x_2}{s} - \arctan\frac{x_1}{s}\right),$$

https://doi.org/10.1017/9781009291200.008 Published online by Cambridge University Press

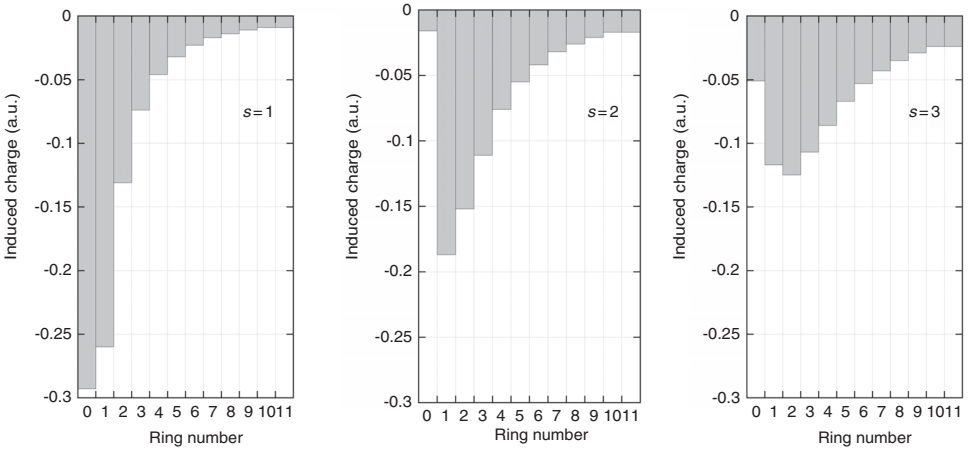

Figure 6.9 Charge induction on concentric rings, for three values of the distance s of the charge.

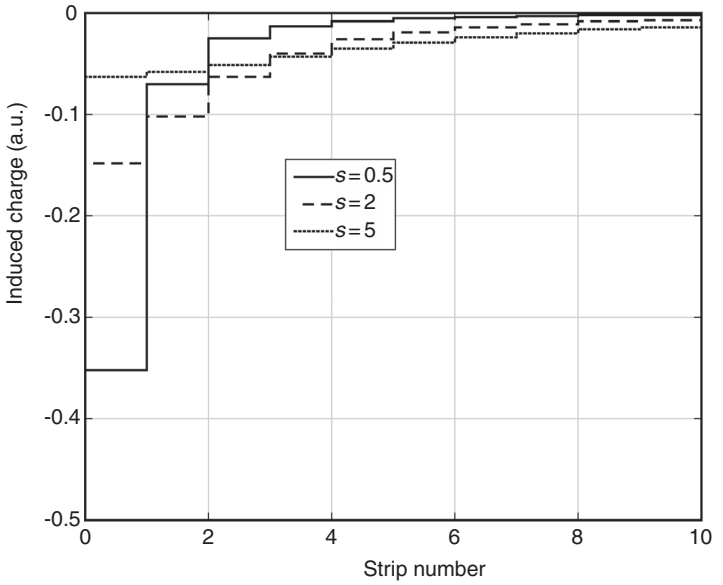

Figure 6.10 Charge induction on parallel strips, for several values of the distance of the charge.

which represents the incremental charge induction on a set of parallel strips; Figure 6.10 shows the charge induction profile on ten adjacent strips of unitary length, computed for three values of the distance s.

It is appropriate to note that all expressions and figures given in this section provide the static charge distributions on the electrode surface; the observable

https://doi.org/10.1017/9781009291200.008 Published online by Cambridge University Press

quantity called 'charge induction', generated by the motion of the primary charges, is obtained as the difference between the distributions at different times, and is in general opposite in polarity (see the golden rule of charge induction in Section 6.1).

6.4 Signals induced by the avalanche process

At high electric fields avalanche multiplication sets in, exponentially increasing the number of charges collected and consequently modifying the amplitude and time development of the detected signals. The total number of charges created depends on the field strength, number and distribution within the counter of the original ionization electrons. With reference to Figure 6.2, assume that n_0 electrons of charge e are produced simultaneously at the surface of the upper electrode (the cathode) and start moving towards the anode with a mean free path for multiplication given by α^{-1}, α being the first Townsend coefficient (number of ionizing collisions per unit path length), constant for a fixed value of the field. The rate of increase in the number of electrons due to the multiplication process is then written as:

$$\mathrm{d}n = n\,\alpha\,\mathrm{d}s, \tag{6.13}$$

and their total number after a path s:

$$n = n_0 \mathrm{e}^{\alpha s}, \tag{6.14}$$

the ratio between final and total charge, $M = n/n_0$, is the gain of the counter.

The differential charge induction due to the multiplying electrons when they reach the position s is therefore (from expression (6.1)):

$$\mathrm{d}q^- = en_0\,\mathrm{e}^{\alpha s}\frac{\mathrm{d}s}{s_0};$$

an integration provides the total induced charge at the same position:

$$q^-(s) = \frac{en_0}{\alpha s_0}(\mathrm{e}^{\alpha s} - 1) \cong \frac{en_0}{\alpha s_0}\mathrm{e}^{\alpha s}, \tag{6.15}$$

or, as a function of the time from the start of the avalanche:

$$q^-(t) = \frac{en_0}{\alpha s_0}(\mathrm{e}^{\alpha w^- t} - 1) \cong \frac{en_0}{\alpha s_0}\mathrm{e}^{\alpha w^- t}, \tag{6.16}$$

where w^- is the drift velocity of the avalanching electrons. The corresponding current is obtained by differentiation:

$$i^-(t) = \frac{en_0 w^-}{s_0}\mathrm{e}^{\alpha w^- t} = \frac{en_0}{T^-}\mathrm{e}^{\alpha w^- t} \quad (t \le T^-) \tag{6.17}$$

https://doi.org/10.1017/9781009291200.008 Published online by Cambridge University Press

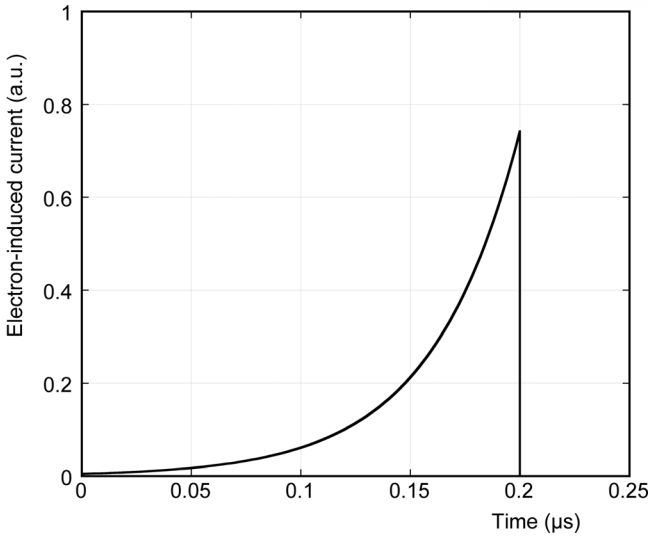

Figure 6.11 Electron-induced current by an avalanche on the cathode.

where T^- is the total collection time for the electrons in the avalanche. One can see from expression (6.15) that after full collection ($s = s_0$), the total charge induced by the electrons, the so-called fast signal in an avalanche counter, corresponds to only a fraction of the total charge generated in the avalanche:

$$q^-(T^-) \cong \frac{en_0}{\alpha s_0} \mathrm{e}^{\alpha s_0}. \tag{6.18}$$

It is a common mistake, when using amplifiers with short differentiation constants (therefore only detecting the fast electron component of the signal), to underestimate the gain of the counter, neglecting the factor αs_0 in the previous expression.

The time evolution of the current induced by the electron component in the avalanche is shown in Figure 6.11 for a typical choice of parameters.

The contribution to the induced charge due to positive ions can also be computed by taking into account the exponential growth in the number of ions during the avalanche process followed by the drift and gradual collection of ions at the cathode. The following expressions can be derived, see for example Raether (1964):

$$\begin{aligned} i^+(t) &= \frac{en_0}{T^+}\left(\mathrm{e}^{\alpha w^- t} - \mathrm{e}^{\alpha w^+ t}\right), \quad (0 \le t \le T^-), \\ i^+(t) &= \frac{en_0}{T^+}\left(\mathrm{e}^{\alpha s_0} - \mathrm{e}^{\alpha w^* t}\right), \quad (T^- \le t \le T^- + T^+), \end{aligned} \tag{6.19}$$

https://doi.org/10.1017/9781009291200.008 Published online by Cambridge University Press

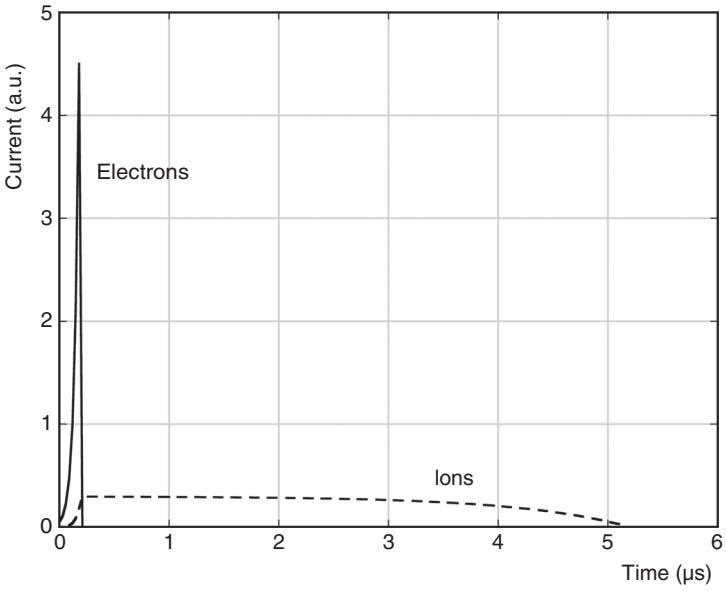

Figure 6.12 Avalanche-induced current on cathodes by electrons and ions.

with

$$\frac{1}{w^*} = \frac{1}{w^+} + \frac{1}{w^-}.$$

The electron and ion induced currents on the cathode are shown in Figure 6.12; the corresponding time evolution of the charge can be computed by integration:

$$q^+(t) = \frac{en_0}{\alpha T^+}\left(\frac{e^{\alpha w^- t}}{w^-} - \frac{e^{\alpha w^* t}}{w^*} + \frac{1}{w^+}\right), \quad (0 \le t \le T^-), \tag{6.20}$$

$$q^+(t) = \frac{en_0}{T^+}\left((t - T^-)e^{\alpha s_0} - \frac{e^{\alpha w^* t} - e^{\alpha w^* T^-}}{\alpha w^*}\right), \quad (T^- \le t \le T^- + T^+).$$

Figure 6.13 shows the total charge induction due to electrons and ions, computed for an unphysical difference by a factor of ten between electron and ion mobility.

In the previous calculations it has been assumed that the initial electron charge released at the surface of the cathode, therefore getting full amplification. In the case of an extended distribution of charge within the gap, as produced by a charged particle traversing the chamber, each electron undergoes an avalanche multiplication by a factor $e^{\alpha s}$, s being its distance from the anode; the resulting signal depends on the density and space distribution of the charges released in the gas. In the particular case of a uniform ionization produced between anode and cathode

https://doi.org/10.1017/9781009291200.008 Published online by Cambridge University Press

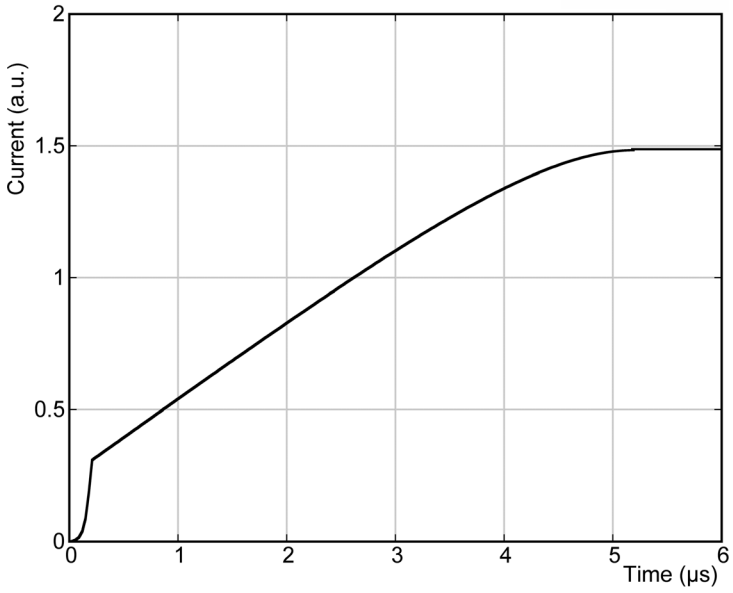

Figure 6.13 Total cathode induced charge by the avalanche multiplication.

with density r, the current induced by the electron component in the avalanche can then be written as (Raether, 1964):

$$i^{-}(t) = \frac{e\rho s_0}{T^{-}} e^{\alpha w^{-} t}\left(1 - \frac{t}{T^{-}}\right), \quad 0 \le t \le T^{-}; \tag{6.21}$$

the maximum signal is obtained after a time $t^{-}_{\max} = T^{-}(1 - 1/\alpha s_0)$ and has a value $i^{-}_{\max} = (e\rho/\alpha s_0)e^{\alpha s_0 - 1}$, as shown in Figure 6.14. Since the avalanche development is much faster than the ions' collection time, the induced ion signal is very similar in shape (but not in amplitude) to the case described previously.

6.5 Grid transparency

Internal wire grids or mesh electrodes mounted between anode and cathode are used often in gaseous detectors for different purposes: screening of the pickup electrode from long signals induced by charges moving in the main drift volume of the detector (the so-called Frisch grid in ionization chambers), intermediate electrodes in the multi-step chamber (Charpak and Sauli, 1978), cathodes of the multiwire chamber end-cap detectors in time projection chambers (Nygren and Marx, 1978), separation from the low drift and the very high avalanche field in Micromegas (Giomataris *et al.*, 1996). It is therefore instructive to estimate the

https://doi.org/10.1017/9781009291200.008 Published online by Cambridge University Press

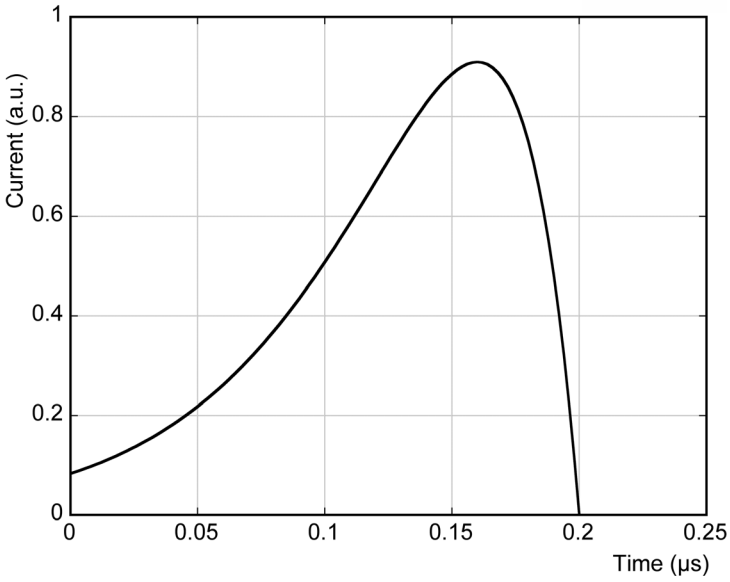

Figure 6.14 Current signal induced on cathodes by an extended track under avalanche multiplication.

transmission efficiency, or electrical transparency, of the electrodes, both for ions and electrons, and the fraction of signal induced through the mesh.

An analytical expression for the electrical transparency of a grid of parallel wires can be obtained by computing the number of field lines intercepted by a mesh inserted between two regions of field E_1 and E_2 (Bunemann *et al.*, 1949):

$$T(E_1, E_2, \rho) = 1 - \frac{1}{\pi E_1}\left[(E_1 + E_2)\sqrt{\rho^2 - \left(\frac{E_2 - E_1}{E_2 + E_1}\right)^2} - (E_2 - E_1)\cos^{-1}\left(\frac{E_2 - E_1}{E_2 + E_1}\frac{1}{\rho}\right)\right], \tag{6.22}$$

with $\rho = 2\pi r/a$, where r and a are, respectively, the radius and distance apart of the wires in the mesh. The equation is only valid in the range of fields where the square root and the inverse cosine are real, namely:

$$\frac{1-\rho}{1+\rho} < \frac{E_2}{E_1} < \frac{1+\rho}{1-\rho}.$$

The quoted work, aimed at optimizing the Frisch grid ionization chamber performance, provides also the electrostatic signal shielding efficiency of a mesh. Figure 6.15 shows the transparency of a mesh as a function of the ratio of fields E_2/E_1 and several values of the parameter ρ. As can be seen, the transparency

https://doi.org/10.1017/9781009291200.008 Published online by Cambridge University Press

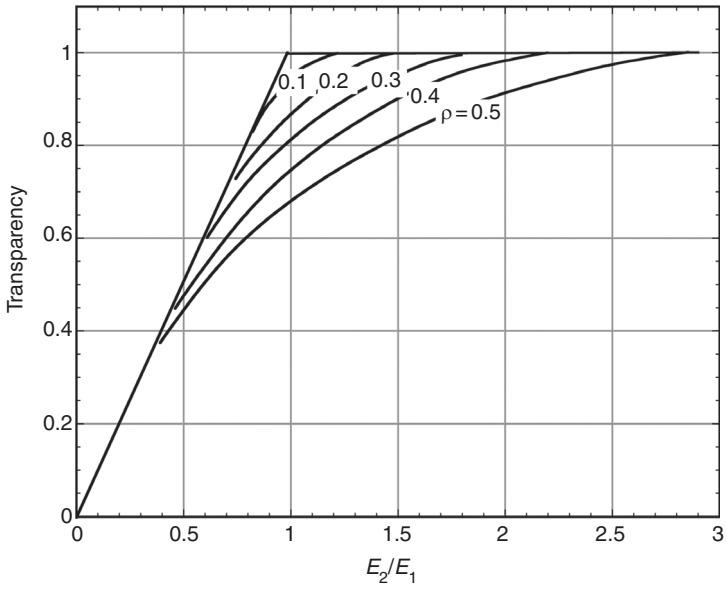

Figure 6.15 Charge transparency of a parallel wire mesh as a function of field ratio and geometry.

increases towards unity with the increasing field ratio; for large values of ρ (thicker or denser wires) full transmission is only reached at large ratios of fields. It should be noted that this calculation does not take into account the diffusion of charges in their drift through the structure, and the consequent capture losses; experimental values tend therefore to be smaller that the calculation.

No theoretical calculations seem to exist for the transparency of a crossed wire mesh, which remains an experimental issue. In a coarse approximation, it can be assumed that the electron transparency in this case is given by the square of the value for the one-dimensional grid.

6.6 Applications of parallel plate avalanche counters (PPACs)

Gaseous counters exploiting the avalanche multiplication between parallel electrodes are easy to build and operate. In the simplest structure with two metal foil electrodes, the avalanche size depends on the position of the primary ionization, and therefore the response of the counter is not proportional to the initial charge. As discussed in Section 6.2, however, the collected charge is proportional to the primary ionization for extended tracks. The cathode foil in a PPAC can be replaced with a semi-transparent mesh, separating the low field drift region from the multiplication gap; the ionization clusters produced in the drift volume are then amplified uniformly, with the detected charge proportional to the energy

https://doi.org/10.1017/9781009291200.008 Published online by Cambridge University Press

deposition; this allows detection and imaging of radiation releasing localized ionization trails, as X-rays or neutrons.

Compared to wire counters, the avalanche multiplication in uniform fields has smaller statistical dispersions, and PPACs have intrinsically a better energy resolution. This can be understood to be a consequence of the fact that, the total gain being equal, in wire counters the mean free path for multiplication gets shorter and shorter on approaching the anode, and a small fluctuation results in large gain variations. A detailed study of the avalanche statistics is given for example by Alkhazov (1970) and Alkhazov (1969) and is discussed in Section 7.5. Since the signal is induced on electrodes immediately after the initial growth of the avalanche, PPACs have also intrinsically a very fast response with sub-ns time resolution, and have been used, for example, in the determination of short nuclear states lifetimes (Krusche *et al.*, 1965).

The major limitation for the use of PPACs is their tendency to discharge when attempting to reach high multiplication factors; because of the large energy stored in the detector, a spark can have very damaging effects both to the detectors and to the readout electronics. The exponential dependence of the gain from the field, and therefore from the gap thickness, demands a very strict tolerance in construction, and sets limits to the size of detectors. Small imperfections on the cathode may

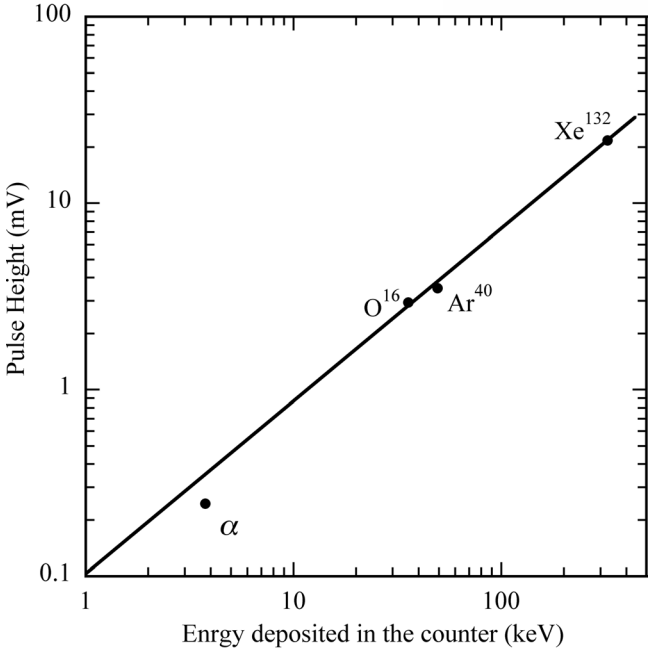

Figure 6.16 Pulse height dependence on energy loss in a PPAC (Stelzer, 1976). By kind permission of Elsevier.

https://doi.org/10.1017/9781009291200.008 Published online by Cambridge University Press

cause the spontaneous emission of electrons, starting an avalanching growth that can exceed the Raether limit and leading to a discharge; although there are examples of use of PPACs for detection of fast particles (Urban *et al.*, 1981), their most common application has been for detection of highly ionizing ions.

The use of resistive electrodes is an effective way to limit the energy flowing in a discharge and allows for safer operation, yet preserving the major performances of the detector (Chtchetkovski *et al.*, 2000); this subject is covered in Chapter 12.

Measured with a medium-size PPAC with a low pressure hydrocarbon gas filling, Figure 6.16 shows the relative pulse height as a function of energy and Figure 6.17 the voltage dependence of gain for ions of different mass and energies (Stelzer, 1976). With low pressure isobutane, time resolutions between two and three hundred ps FWHM have been measured for low energy protons and α particles, Figure 6.18 (Breskin and Zwang, 1977).

The good linearity and proportionality of the detectors, combined with the excellent time resolution, permit the identification of the ions in spectrometers, see for example Sernicki (1983), Hempel *et al.*, (1975) Prete and Viesti (1985). Other applications include the detection of fission fragments and, with an internal converter, of neutrons (Nishio *et al.*, 1997; Jamil *et al.*, 2012).

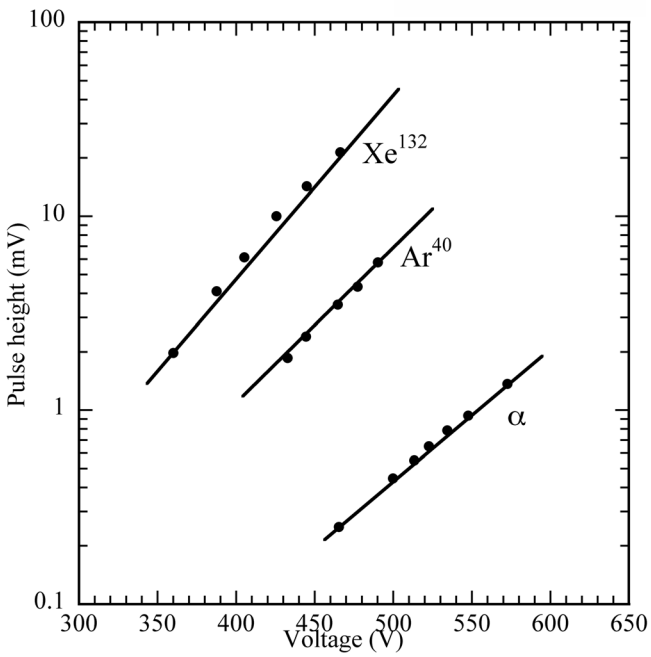

Figure 6.17 Pulse height dependence on voltage for several ions (Stelzer, 1976). By kind permission of Elsevier.

https://doi.org/10.1017/9781009291200.008 Published online by Cambridge University Press

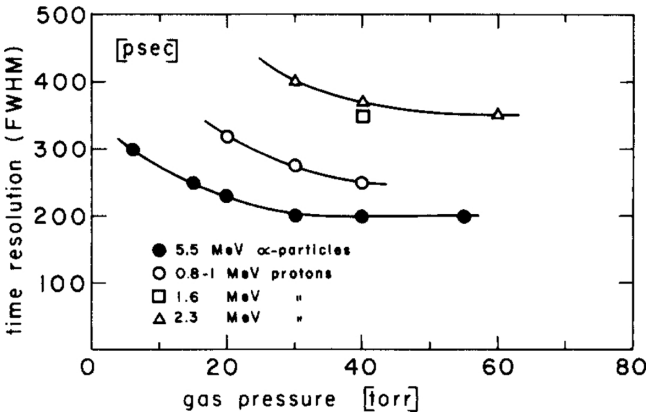

Figure 6.18 PPAC time resolution as a function of i-C_4H_{10} pressure for several ions (Breskin and Zwang, 1977). By kind permission of Elsevier.

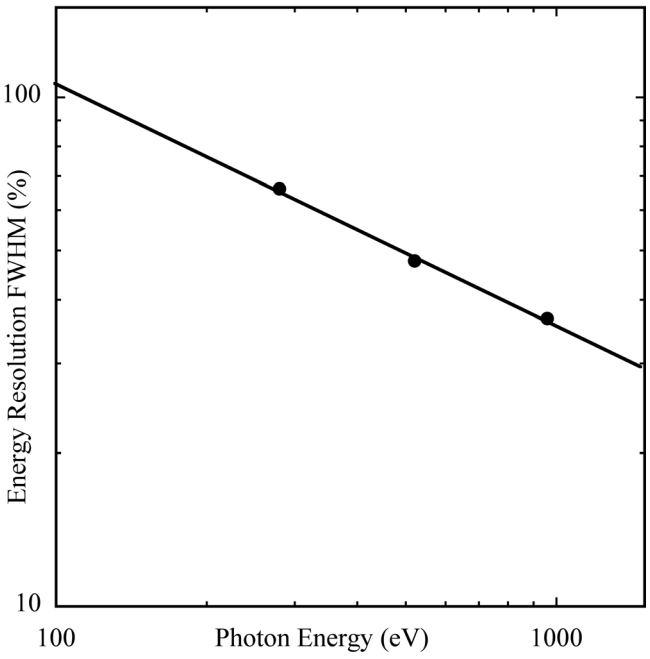

Figure 6.19 Energy resolution of a PPAC as a function of photon energy (gas filling Ar-C_2H_6 at 28 torr) (Smith *et al.*, 1990). By kind permission of Elsevier.

Operation with low pressure hydrocarbon gas fillings, while providing high gains, permits one to use thin entrance windows, suitable for detection of soft X-rays; this detector design has been successfully used, with excellent energy resolution, for fluorescence analysis, as shown for example in Figure 6.19 (Smith *et al.*, 1990).

https://doi.org/10.1017/9781009291200.008 Published online by Cambridge University Press

Used as end-cap detector for large volume drift and time projection chambers, the PPAC has the advantage of reducing the positive ion feedback and increasing the rate capability, as compared to conventional MWPC readout (Peisert, 1983). The Micromegas detector, described in Section 13.3, is of similar conception and, thanks to the use of very thin multiplication gaps, solves many of the gain uniformities problems encountered in standard PPACs.

Parallel electrode multiplying structures are also used in scintillating proportional counters, reaching the statistical limit in energy resolution, see Section 7.6.